

Quantum Transport and Shot Noise in Two-Dimensional Semi-Dirac System

Wei Jie Chan, L. K. Ang,^{a)} and Yee Sin Ang^{a)}

Science, Mathematics and Technology (SMT), Singapore

University of Technology and Design (SUTD), 8 Somapah Road,

Singapore 487372

Two-dimensional (2D) semi-Dirac systems, such as 2D black phosphorus and arsenene, can exhibit a rich topological phase transition between insulating, semi-Dirac, and band inversion phases when subjected to an external modulation. How these phase transitions manifest within the quantum transport and shot noise signatures remain an open question thus far. Here, we show that the Fano factor converges to the universal $F \approx 0.179$ at the semi-Dirac phase, and transits between the sub-Poissonian ($F \approx 1/3$) and the Poissonian shot noise ($F \approx 1$) limit at the band inversion and the insulating phase, respectively. Furthermore, the conductance of 2D semi-Dirac system converges to the contrasting limit of $G/G_0 \rightarrow 1/d$ and $G/G_0 \rightarrow 0$ at the band inversion and the insulating phases, respectively. The quantum tunneling spectra exhibits a peculiar coexistence of massless and massive Dirac quasiparticles in the band inversion regime, thus providing a versatile sandbox to study the tunneling behavior of various Dirac quasiparticles. These findings reveal the rich interplay between band topology and quantum transport signatures, which may serve as smoking gun signatures for the experimental studies of semi-Dirac systems near topological phase transition.

^{a)} Authors to whom correspondence should be addressed: ricky_ang@sutd.edu.sg and yeesin_ang@sutd.edu.sg

Shot noise is generated by electrical current fluctuations arising from the discrete nature of charge carriers. Shot noise can be used as an indicator of the correlation between charged carriers¹⁻⁴. A well-known characterization of shot noise is the Fano factor, F , which is defined as the ratio between the actual shot noise and the Poisson shot noise with $F = 1$. Prominent examples of systems with $F \neq 1$ include the super-Poissonian shot noise with $F > 1$ in zero-dimensional quantum dots^{5,6} and the sub-Poissonian shot noise with $F = 1/3$ in both disordered conductors^{7,8} and graphene⁹⁻¹¹. Furthermore, the well-celebrated maximal Fano factor value in graphene is shown to be associated with the minimal conductivity in orders of e^2/h ⁹. Importantly, shot noise provides a useful tool to probe the quantum transport properties of an electronic system¹², and has been widely employed in the experimental studies of graphene and their heterostructures^{13,14}.

Two-dimensional (2D) semi-Dirac material (SDM) represents an interesting system that simultaneously host linear (relativistic) energy dispersion in one direction and parabolic (nonrelativistic) energy dispersion in the orthogonal direction¹⁵⁻¹⁷. SDMs has been realized in a large variety of systems, including $(\text{TiO}_2)_m/(\text{VO}_2)_n$ nanostructure¹⁸, strained organic salt¹⁹, photonic crystals²⁰, $\text{Bi}_{1-x}\text{Sb}_x$ ²¹, striped boron sheet²², on surface states of topological insulators^{23,24}, or in non-centrosymmetric systems²⁵ such phosphorus-based materials²⁶⁻³², monolayer arsenene³³, silicene oxide³⁴, and polariton lattice³⁵ and also shown in α -dice lattice³⁶⁻³⁸ with higher pseudospin. The electronic transport and shot noise of SDM have been studied extensively in previous works, which establish a Fano factor of $F = 1$ and $F \approx 0.179$ at the band insulator phase with nonzero band gap and at the semimetallic gapless limit, respectively³⁸⁻⁴⁷. Nevertheless, 2D SDM can undergo complex topological phase transitions. Beyond the band insulating and the semimetallic regime, SDM can exhibit a band inversion phase²⁵ in which two distinct Dirac cones emerge, thus rendering the band-inverted SDM a strong potential for valleytronic device applications⁴⁵. Nevertheless, the shot noise and conductance signatures of band-inverted SDM remains an open question thus far.

In this work, we study the quantum transport of SDM near the topological phase transitions. Focusing on the quantum transport occurring along the relativistic direction - not covered in previous quantum transport study⁴⁵, we observe the intriguing coexistence of massless^{9,48} and massive Dirac fermions in the tunneling spectra at fixed transport channel at all quasiparticle energies, which is distinctive from that of bilayer graphene⁴⁹ in which

the massive and massless Dirac quasiparticle occurs at various transversal momenta at different quasiparticle energies. We further calculate the conductance and Fano factors of 2D SDMs as the band topology changes continuously from band insulating to band inversion phases. Remarkably, we found that the Fano factor converges to sub-Poissonian shot noise with $F \approx 1/3$ and to Poissonian shot noise with $F \approx 1$ in the band inversion and insulating phase, respectively [Fig. 1(a)]. Such shot noise signatures have negligible thermal noise contributions, even at room temperature. Our findings reveal the exotic quantum transport behavior and the shot noise signatures of 2D SDM at various phases, thus uncovering shot noise as a useful tool in probing the band topology of 2D SDM.

2D SDM can be described by a two-band effective Hamiltonian^{50,51},

$$\hat{H} = (\alpha k_x^2 + \Delta) \sigma_x + \beta k_y \sigma_y, \quad (1)$$

with $\alpha = \hbar^2/(2m^*)$ and $\beta = \hbar v_y$, where m^* and v_y being the effective mass along \hat{x} and Fermi velocity along \hat{y} , respectively. A phase transition parameter, Δ , acts as a perturbation factor that continuously changes the band topology from band insulating phase ($\Delta > 0$), semi-Dirac phase ($\Delta = 0$) to band inversion phase ($\Delta < 0$). We can nondimensionlise Eq. (1) by defining the characteristic momentum and energy ($\hbar k_0 = 2m^*v_y$ and $\varepsilon_0 = \hbar k_0 v_y$) to obtain $\hat{\mathcal{H}} = (k_x^2 + \Delta) \sigma_x + k_y \sigma_y$ which has the following energy dispersion

$$\varepsilon_{\mathbf{k}} = \pm \sqrt{(k_x^2 + \Delta)^2 + k_y^2}, \quad (2)$$

where \pm indicates conduction/valence (+/-) bands. This parameter has been utilized for directional dependent transport^{40,52-56} and phase-dependent transport^{36,44,57,58}. Owing to the presence of two inequivalent valleys in the band inversion phase ($\Delta < 0$), band-inverted 2D SDMs have been widely studied for potential applications in valleytronics⁴⁴⁻⁴⁷.

From Fig. 1(a), the SDM ($\Delta = 0$) with a semi-Dirac point at $(k_x, k_y) = (0, 0)$ can become a band insulator ($\Delta > 0$) or exhibit a band inversion ($\Delta < 0$) phase with band crossings at $(k_x, k_y) = (\pm k_D, 0)$, with $k_D = \sqrt{|\Delta|}$ ^{15,17,25}. Interestingly, Eq. (1) in the band inversion regime can be decomposed into either the 1D massless and massive Dirac Hamiltonian [Fig. 1(c)] along the k_y direction at $k_x = \pm k_D$ and at $k_x = 0$, respectively,

$$\hat{H}(\Delta < 0) = \begin{cases} k_y \sigma_y, & k_x = \pm k_D; \\ \Delta \sigma_x + k_y \sigma_y, & k_x = 0. \end{cases} \quad (3)$$

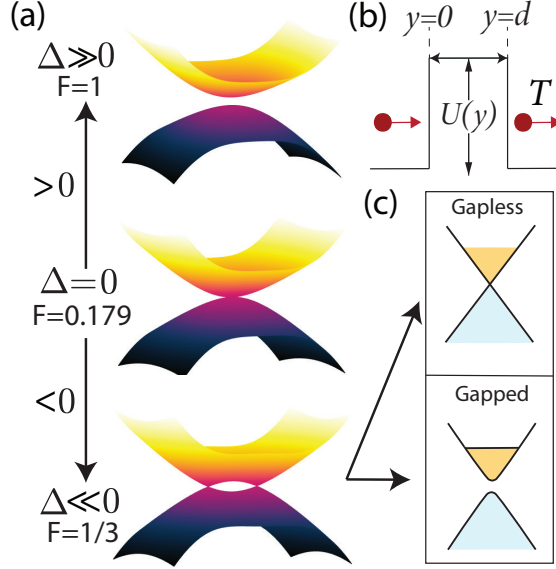


FIG. 1: Illustration of the insulating ($\Delta > 0$), semi-Dirac ($\Delta = 0$) and band inversion ($\Delta < 0$) phase tuned by Δ in Eq. (1) with its corresponding Fano factors in (a). Illustration of chiral tunneling across a potential barrier with width d and transmission probability T along the linear dispersion (k_y) in (b). The band inversion phase in (a) can co-exhibit both gapless/gapped band crossings along k_y depending on its transverse momenta, k_x in (c).

The quantum transport along the k_y direction is thus expected to exhibit a mixture of massive and massive Dirac quasiparticles dictated by Eq. (3).

The transmission probability T can be obtained by considering a scattering potential along k_y [Fig. 1(b)] with $U(y) = \mathcal{U}_0(\Theta(y) - \Theta(y - d))$, where $U_0 \equiv \mathcal{U}_0/\varepsilon_0$ and $d \equiv d_0 k_0$ are the dimensionless potential height/barrier width respectively. In the $L_x \gg d$ limit, the Hamiltonian decouples into a 1D eigenvalue equation along $k_y \rightarrow -i\partial_y$, with

$$\Psi_j = A_j \begin{pmatrix} \varepsilon_j \\ k_x^2 + \Delta + ik_j \end{pmatrix} e^{ik_j y} + B_j \begin{pmatrix} \varepsilon_j \\ k_x^2 + \Delta - ik_j \end{pmatrix} e^{-ik_j y}, \quad (4)$$

where the index j denotes the L (left), B (barrier), and (R) right region. The energy and wavevector with index j denotes $\varepsilon_{L/R} = \varepsilon_{\mathbf{k}}$, $\varepsilon_B = \varepsilon_{\mathbf{k}} - U_0 \equiv \varepsilon_{\mathbf{q}}$ with $k_{L/R} = k_y = \lambda \sqrt{\varepsilon_{\mathbf{k}}^2 - (k_x^2 + \Delta)^2}$, $k_B = q_y = \lambda' \sqrt{\varepsilon_{\mathbf{q}}^2 - (k_x^2 + \Delta)^2}$, $\lambda = \text{sgn}(\varepsilon_{\mathbf{k}})$ and $\lambda' = \text{sgn}(\varepsilon_{\mathbf{q}})$. For the left incident wavefunction, $A_L = 1$ and $B_R = 0$ are enforced with the transmission coefficient $t = A_R$. For only forward-moving electronic states in region R, the wavevectors are enforced in Eq. (4) through $k_y > 0$ and $q_y < 0$. For n - p - n junction, the conservation of current (non-dimensionlized), $\hat{J}_i + \hat{J}_r = \hat{J}_t$ with $\hat{J}_y = \frac{\hbar}{2} \Psi^\dagger \hat{\sigma}_y \Psi = \frac{\hbar}{2} \Psi^\dagger \hat{\sigma}_y \Psi$, gives us the relation

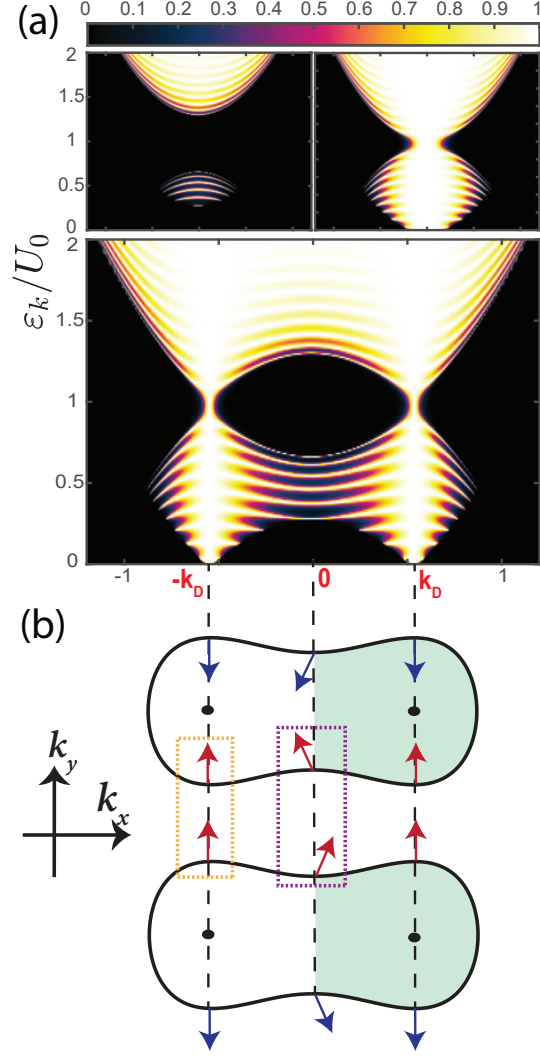


FIG. 2: Transmission probability T for $\Delta = 0.3, 0$ and -0.3 are shown in the top left/top right/bottom panels in (a). Pseudospin vectors from Eq. (6) are shown in (b) with red/blue arrows indicating the the direction of S_y .

$|r|^2 + |t|^2 = 1$. By matching the boundary conditions at $y = 0$ and d , we obtain $T = |t|^2$ as

$$T = \frac{4\varepsilon_{\mathbf{k}}^2 \varepsilon_{\mathbf{q}}^2 k_y^2 q_y^2}{4\varepsilon_{\mathbf{k}}^2 \varepsilon_{\mathbf{q}}^2 k_y^2 q_y^2 \cos^2(\lambda' q_y d) + \sin^2(\lambda' q_y d) [(k_x^2 + \Delta)^2 U_0^2 + \varepsilon_{\mathbf{k}}^2 q_y^2 + \varepsilon_{\mathbf{q}}^2 k_y^2]^2}, \quad (5)$$

in agreement with a band insulator for $\Delta > 0$ [top left panel of Fig. 2(a)] and a SDM⁴⁰ for $\Delta = 0$ by noticing that $\tan \phi = (k_x^2 + \Delta)/k_y$ and $\tan \theta = (k_x^2 + \Delta)/q_y$ [top right panel of Fig. 2(a)]. Remarkably, the rotational invariant of Eq. (2) around \hat{z} , i.e. $[H, R_z] = 0$ with R_z being a rotation operator about the \hat{z} , allows Eq. (5) to fully capture the Klein

tunneling behavior, as evident under rotation and incident angle^{39,43}. However, this cannot be generalized along the parabolic direction due to intervalley scattering^{39–41,45}.

We now focus on the band inversion phase for $\Delta < 0$ [bottom panel of Fig. 2(a)]. The tunneling behavior³⁷ in Eq. (5) at different transverse momenta, k_x , can be understood from the pseudospin texture⁴⁵ (non-dimensionalized) shown in Fig. 2(b) and is given by

$$\mathbf{S} = \Psi^\dagger \boldsymbol{\sigma} \Psi = \left(\frac{k_x^2 + \Delta}{\varepsilon_{\mathbf{k}}}, \lambda \frac{k_y}{\varepsilon_{\mathbf{k}}} \right). \quad (6)$$

As T is symmetric about k_x [green shading in the lower half contours], it suffices to analyze the non-positive transverse momenta with $k_x \leq 0$. At a Dirac point $k_x = -k_D$, the conservation of pseudospin across the potential barrier [orange dotted box] enables Klein tunneling at normal incidence with $T = 1$ [Fig. 2(a)], which resembles the 1D tunneling of massless Dirac fermions at $k_x = -k_D$ in Eq. (1). Similarly, transmission resonances occur at $0 \leq k_x < k_D$ [purple box in Fig. 2(a)], which resembles the 1D tunneling of gapped massive Dirac fermions.

As illustrated in Eq. (3), there exist two special transport channel at $k_x = k_D$ in which the quasiparticles tunnel with full transmission. Such Klein tunneling behavior arises because of the 1D gapless massive Dirac Hamiltonian at $k_x = k_D$ [see Eq. (3)]. At $k_x = 0$, the effective 1D Hamiltonian [Eq. (3)] reduces to that of a gapped Dirac quasiparticle. The tunneling spectra at the transport channel of $k_x = 0$ thus deviates from perfect Klein tunneling and exhibits oscillations instead. It should be noted that the coexistence of massive and massless Dirac fermions have also been reported in twisted bilayer graphene⁴⁹. However, in twisted bilayer graphene, the massive and massless Dirac quasiparticles occur at different transport channel (i.e. transversal momenta) dependent on the energy of the quasiparticles. This aspect is in stark contrast to the case of 2D SDM studied here, in which the massless and massive Dirac quasiparticles occur at *fixed* transport channels of $k_x = k_D$ and $k_x = 0$, respectively.

The modulation of pseudogap through U_0 and Δ is shown in Fig. 3(a). While the full transmission, oscillatory and pseudogap regions are expected from Klein tunneling^{9,49}, an abrupt cutoff for $\varepsilon_{\mathbf{k}} = 0.5$ at $\Delta = 0.5$ is observed. This is attributed by the crossover of the incident wavefunction from propagating to evanescent when $k_y = \sqrt{\varepsilon_{\mathbf{k}}^2 - \Delta^2}$ becomes imaginary at $k_x = 0$. This implies that the cutoff for $\varepsilon_{\mathbf{k}} = 1.5$ appears only at $\Delta = -1.5$. Hence, the decoupling of the band inversion phase with $\Delta \ll 0$, in the semi-Dirac

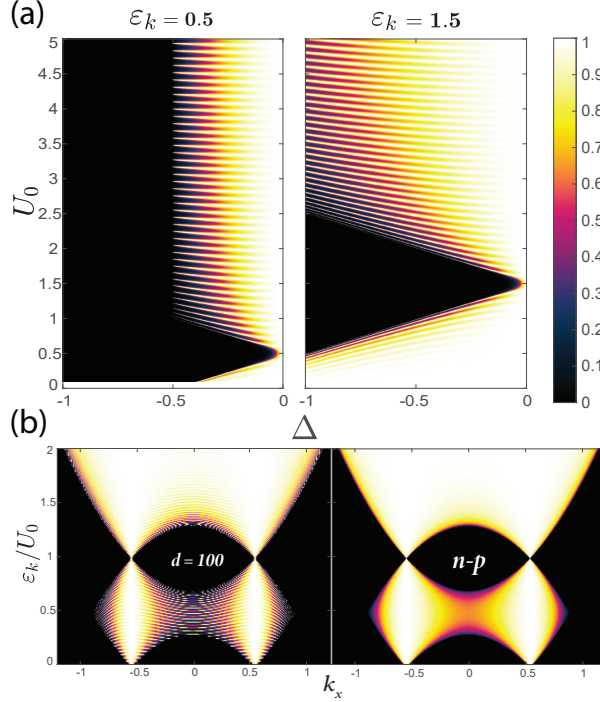


FIG. 3: The relationship of U_0 against Δ on T are plotted in (a) with both $\varepsilon_{\mathbf{k}} = 0.5$ and 1.5. The effects of potential barrier width d on T are shown in (b) for $d = 100$ and in the $n-p$ limit at $\Delta = -0.3$.

literatures^{37,50,51} can be attributed to the crossover of propagating to evanescent incident wavefunction.

The retention of the Klein tunneling behavior from $d = 30$ [Fig. 2(a)] to $d = 100$, and subsequently to the $n-p$ limit is in Fig. 3 by setting $t = A_B$, $A_R = B_R = 0$ in Eq. (4) s.t.

$$T_{np} = \frac{4\lambda'q_yk_y\varepsilon_{\mathbf{q}}\varepsilon_{\mathbf{k}}}{\lambda(|\lambda k_y\varepsilon_{\mathbf{q}} + \lambda'\varepsilon_{\mathbf{k}}q_y|^2 + U_0^2(k_x^2 + \Delta)^2)}, \quad (7)$$

with the conservation of pseudospin dictating $|r|^2 + |t|^2\lambda'q_y\varepsilon_{\mathbf{k}}/(\lambda k_y\varepsilon_{\mathbf{q}}) = 1$ and by neglecting the evanescent wave contributions.

We now investigate the quantum transport signatures, i.e., conductance G and Fano factor F [Fig. 4]. In the zero-temperature limit, G and F can be expressed as

$$G = G_0 \int T dk_x; \quad F = \frac{S_I}{G}, \quad (8)$$

with $G_0 = ge^2/(2\pi h)$, g is the degeneracy term (spin and valley), e is the electronic charge, h is the Planck's constant, $S_I = \int T(1 - T)dk_x$ is the current noise and T is obtained from

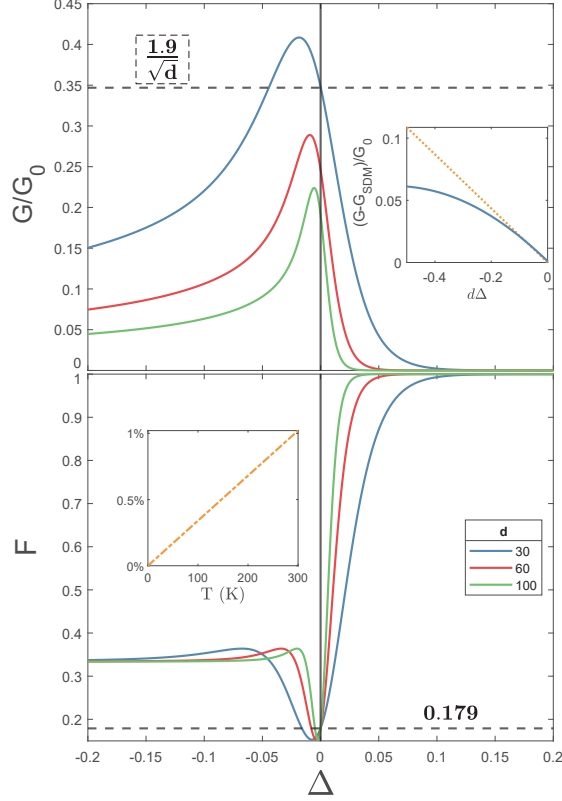


FIG. 4: The conductance G/G_0 (top) and Fano factor F (bottom) [Eq. (8)] are plotted respectively across Δ with $d = 30$ (blue), $d = 60$ (red) and $d = 100$ (green). (Top): The broken line is the SDM conductance value, i.e. $G_{SDM}/G_0 = 1.9/\sqrt{d}$. The top inset shows the relationship between $(G - G_{SDM})/G_0$ (blue solid line) with $d = 30$ against its linear approximation (orange dotted line) with $-0.5 \leq d\Delta \leq 0$ in the band inversion phase. (Bottom): The broken line is the SDM Fano factor, i.e. $F \approx 0.179$. The bottom inset shows the thermal noise correction up to 300K for all Δ .

Eq. (5) in the grazing energy ($\varepsilon_{\mathbf{k}}/U_0 \rightarrow \gg 1$) and tall barrier ($L_x \gg d$) limit⁹ s.t.

$$T \rightarrow \text{sech}^2((k_x^2 + \Delta)d), \quad (9)$$

with $\varepsilon_{\mathbf{k}} \rightarrow U_0$, $\varepsilon_{\mathbf{q}} \rightarrow 0$, $q_y^2 \rightarrow -(k_x^2 + \Delta)^2$, and $k_y^2 \rightarrow U_0^2 - (k_x^2 + \Delta)^2$.

The conductance G/G_0 and the Fano factor F at $d = 30$ (blue), $d = 60$ (red) and $d = 100$ (green) are shown in Fig. 4. Away from the semi-Dirac point with $(G/G_0 \approx 1.9/\sqrt{d}$, $F \approx 0.179)$ ⁴⁰, the values converge towards the insulating ($\Delta > 0$) with $(G/G_0 = 0, F \rightarrow 1)$ and band inversion ($\Delta < 0$) phase with $(G/G_0 = 1/d$ [see inset of top figure], $F \rightarrow 1/3)$ ⁹ respectively. Strikingly, the convergence of the band inversion phase to the sub-Poissonian

TABLE I: Calculated Δ and Fano factors F using material parameters from semi-Dirac materials with $\alpha \sim 1/m^*$, $\beta \sim v_y$, $k_0 \sim m^*v_x$ and $\varepsilon_0 \sim m^*v_x^2$ in Eq. (1). Both the Δ/ε_0 and F values are taken from the insulating and band inversion phase and are calculated using $d = 30$ s.t. the width is approximately 2 to 10 nm.

Material	Method	m^* (m_e)	(v_x, v_y) (10^6m/s)	k_0 (\AA^{-1})	ε_0 (eV)	Δ/ε_0	F
Black P ^{26,29}	Doping	1.42	(0.86, 0.28-0.56 ^a)	1.37	5.065	(0.036, -0.006)	(0.733, 0.154)
5L black P ^{26,27}	E-Field	1.2	(0.202, 0.253)	0.436	0.580	(0.483, -0.362 ^b)	(1, 0.334)
Bilayer P ^{31,59}	Strain	1.25	(0.562, 0.75 ^c)	0.607	1.545	(0.044, -0.03)	(0.822, 0.27)

^a Values from both the insulating and band inversion phase²⁶

^b Linearly extrapolated from insulating phase²⁷

^c Approximated from single layer fermi velocities⁶⁰

value in graphene⁹ and disordered metals^{7,8} can be understood by observing that Eq. (9) captures only the carriers along the $\varepsilon_{\mathbf{k}}/U_0 \approx 1$ line [see Fig. 2(a)]. However, this breaks down in the n - p limit with vanishing T .

G in Eq. (8) can be conveniently utilized as a litmus test of the underlying band structure by linearly expanding Eq. (9) around the semi-Dirac phase ($\Delta = 0$) with $T \approx T(\Delta = 0) - \tilde{T}$ where $T(\Delta = 0)$ is the tunneling probability at the semi-Dirac point, and

$$\tilde{T} = 2d\Delta \tanh(k_x^2 d) \operatorname{sech}^2(k_x^2 d). \quad (10)$$

Correspondingly, the deviation of G away from around the semi-Dirac point with universal conductance $G_{\text{SDP}}/G_0 = 1.9/\sqrt{d}$ is:

$$\frac{G - G_{\text{SDP}}}{G_0} \approx -2d\Delta \int (\tanh(k_x^2 d) \operatorname{sech}^2(k_x^2 d)) dk_x. \quad (11)$$

The range of validity of Eq. (11) [orange dotted line] against the actual deviation, i.e. $(G - G_{\text{SDP}})/G_0$ [blue solid line] at $d = 30$ is shown in the top figure inset of Fig. 4.

Elevated temperature can affect noise measurement by broadening the current fluctuations through thermal excitation, which effectively increase the current noise, S_I and F by approximately 1% at $T = 300\text{K}$ [inset of Fig. 4 in bottom figure]. This is accounted by the measured averaged Fano factor \mathcal{F} , which deviates from the true F with the inclusion of the

Δ -invariant thermal noise⁶¹ s.t.

$$\mathcal{F} \approx \left(\coth \left(\frac{U_0}{2k_B T} \right) - \frac{2k_B T}{U_0} \right) F, \quad (12)$$

where U_0 plays the role of eV here, with V being the applied voltage. This approximation reduces to $S_T = 4k_B T G = 0.0082 < 1\%$ if T is highly dependent on $\varepsilon_{\mathbf{k}}$ [see Eq. (5)] and $eV = U_0 \ll k_B T$. Hence, the miniature contributions of the thermal noise in systems govern by Eq. (1) removes the need for filtering thermal noise in electronics noise measurements as $\mathcal{F} \approx F$.

The F values for SDMs in Table I are calculated using Eq. (8) with the extracted material coefficients. Finally, we briefly comment on the experimental relevance of the model parameter, Δ , which plays the important role in determining the band topology of 2D SDMs. The Δ term can be externally tuned by a large variety of methods, such as varying the dopant distance²⁶, doping density²⁹, applied electric field^{26,27} or strain^{31,34,50,59}. However, cautionary measures should be taken to preserve the space-time inversion symmetry⁶² to observe the phase transitions. Counterexamples are observed either by straining perpendicular to the valleys³¹ or lacking the required symmetry such as in monolayer arsenene or non Tb-stacked phosphorous^{22,33}.

In conclusion, we study the quantum transport and shot noise signature of a 2D semi-Dirac system along the relativistic dispersion direction. The quantum tunneling spectrum exhibits a peculiar coexistence of massless and massive Dirac quasiparticles with full and oscillating transmission probabilities, respectively. 2D semi-Dirac system thus offer a versatile material platform to study the Klein tunneling phenomena.

We further obtain the ballistic tunneling conductance G and the Fano factors F values across different Δ , namely ($G/G_0 \rightarrow 1/d$, $F \approx 1/3$), ($G/G_0 \rightarrow 1.9/\sqrt{d}$, $F \approx 0.179$ and ($G/G_0 \rightarrow 0$, $F \approx 1$) for the band inversion, semi-Dirac, and the band insulating phases, respectively. The conductance and shot noise shall provide useful signatures to experimentally probe the phase transitions of a 2D semi-Dirac system.

W.J.C acknowledge MOE PhD RSS. Y.S.A is supported by the Singapore Ministry of Education Academic Research Fund Tier 2 (MOE-T2EP50221-0019). L.K.A is supported by A*STAR AME IRG (A2083c0057).

AUTHOR DECLARATION

Conflict of Interest

The authors have no conflicts to disclose.

Author Contributions

Wei Jie Chan: Investigation (lead); Methodology (equal); Writing original draft (lead). **Lay Kee Ang:** Supervision (equal); Writing-review & editing (equal). **Yee Sin Ang:** Conceptualization (lead); Methodology (equal); Supervision (equal); Writing-review & editing (equal).

Data Availability

The data that support the findings of this study are available from the corresponding author upon reasonable request.

REFERENCES

- ¹L. S. Levitov and G. B. Lesovik, “Charge distribution in quantum shot noise,” *Jetp Lett. C/C Pis’Ma V Zhurnal Eksp. Teor. Fiz.* **58**, 230 (1993).
- ²Y. Blanter and M. Büttiker, “Shot noise in mesoscopic conductors,” *Phys. Rep.* **336**, 1–166 (2000).
- ³S. Ghosh, H. Surdi, F. Kargar, F. A. Koeck, S. Rumyantsev, S. Goodnick, R. J. Nemanich, and A. A. Balandin, “Excess noise in high-current diamond diodes,” *Appl. Phys. Lett.* **120**, 062103 (2022).
- ⁴D. Chevallier, T. Jonckheere, E. Paladino, G. Falci, and T. Martin, “Detection of finite-frequency photoassisted shot noise with a resonant circuit,” *Phys. Rev. B* **81**, 205411 (2010).
- ⁵E. Onac, F. Balestro, B. Trauzettel, C. F. Lodewijk, and L. P. Kouwenhoven, “Shot-noise detection in a carbon nanotube quantum dot,” *Phys. Rev. Lett.* **96**, 026803 (2006).

- ⁶M. C. Harabula, V. Ranjan, R. Haller, G. Fülöp, and C. Schönenberger, “Blocking-state influence on shot noise and conductance in quantum dots,” *Phys. Rev. B* **97**, 115403 (2018).
- ⁷K. Nagaev, “On the shot noise in dirty metal contacts,” *Phys. Lett. A* **169**, 103–107 (1992).
- ⁸C. W. J. Beenakker and M. Büttiker, “Suppression of shot noise in metallic diffusive conductors,” *Phys. Rev. B* **46**, 1889(R) (1992).
- ⁹J. Tworzydło, B. Trauzettel, M. Titov, A. Rycerz, and C. W. J. Beenakker, “Sub-Poissonian Shot Noise in Graphene,” *Phys. Rev. Lett.* **96**, 246802 (2006).
- ¹⁰R. Danneau, F. Wu, M. F. Craciun, S. Russo, M. Y. Tomi, J. Salmilehto, A. F. Morpurgo, and P. J. Hakonen, “Shot noise measurements in graphene,” *Solid State Commun.* **149**, 1050–1055 (2009).
- ¹¹R. Danneau, F. Wu, M. F. Craciun, S. Russo, M. Y. Tomi, J. Salmilehto, A. F. Morpurgo, and P. J. Hakonen, “Shot Noise in Ballistic Graphene,” *Phys. Rev. Lett.* **100**, 196802 (2008).
- ¹²C. Beenakker and C. Schönenberger, “Quantum shot noise,” *Physics Today* **56**, 37–42 (2003).
- ¹³M. R. Sahu, A. K. Paul, A. Soori, K. Watanabe, T. Taniguchi, S. Mukerjee, and A. Das, “Enhanced shot noise at bilayer graphene–superconductor junction,” *Phys. Rev. B* **100**, 235414 (2019).
- ¹⁴N. Kumada, F. Parmentier, H. Hibino, D. Glattli, and P. Roulleau, “Shot noise generated by graphene p-n junctions in the quantum hall effect regime,” *Nature communications* **6**, 8068 (2015).
- ¹⁵S. Banerjee, R. R. Singh, V. Pardo, and W. E. Pickett, “Tight-binding modeling and low-energy behavior of the semi-dirac point,” *Phys. Rev. Lett.* **103**, 016402 (2009).
- ¹⁶S. Banerjee and W. E. Pickett, “Phenomenology of a semi-Dirac semi-Weyl semimetal,” *Phys. Rev. B* **86**, 075124 (2012).
- ¹⁷H. Huang, Z. Liu, H. Zhang, W. Duan, and D. Vanderbilt, “Emergence of a chern-insulating state from a semi-dirac dispersion,” *Phys. Rev. B* **92**, 161115(R) (2015).
- ¹⁸V. Pardo and W. E. Pickett, “Half-metallic semi-dirac-point generated by quantum confinement in TiO₂/VO₂ nanostructures,” *Phys. Rev. Lett.* **102**, 166803 (2009).
- ¹⁹S. Katayama, A. Kobayashi, and Y. Suzumura, “Pressure-induced zero-gap semiconducting state in organic conductor α -(BEDT–TTF)₂I₃ salt,” *J. Phys. Soc. Japan* **75**, 054705

- (2006).
- ²⁰Y. Wu, “A semi-Dirac point and an electromagnetic topological transition in a dielectric photonic crystal,” *Opt. Express* **22**, 1906 (2014).
- ²¹S. Tang and M. S. Dresselhaus, “Constructing a large variety of Dirac-cone materials in the Bi 1-xSbx thin film system,” *Nanoscale* **4**, 7786–7790 (2012).
- ²²H. Zhang, Y. Xie, Z. Zhang, C. Zhong, Y. Li, Z. Chen, and Y. Chen, “Dirac Nodal Lines and Tilted Semi-Dirac Cones Coexisting in a Striped Boron Sheet,” *J. Phys. Chem. Lett.* **8**, 1707–1713 (2017).
- ²³Q. Li, P. Ghosh, J. D. Sau, S. Tewari, and S. Das Sarma, “Anisotropic surface transport in topological insulators in proximity to a helical spin density wave,” *Phys. Rev. B* **83**, 085110 (2011).
- ²⁴F. Zhai, P. Mu, and K. Chang, “Energy spectrum of dirac electrons on the surface of a topological insulator modulated by a spiral magnetization superlattice,” *Phys. Rev. B* **83**, 195402 (2011).
- ²⁵S. Park and B.-J. Yang, “Classification of accidental band crossings and emergent semimetals in two-dimensional noncentrosymmetric systems,” *Phys. Rev. B* **96**, 125127 (2017).
- ²⁶S. S. Baik, K. S. Kim, Y. Yi, and H. J. Choi, “Emergence of Two-Dimensional Massless Dirac Fermions, Chiral Pseudospins, and Berrys Phase in Potassium Doped Few-Layer Black Phosphorus,” *Nano Lett.* **15**, 7788–7793 (2015).
- ²⁷B. Ghosh, B. Singh, R. Prasad, and A. Agarwal, “Electric-field tunable Dirac semimetal state in phosphorene thin films,” *Phys. Rev. B* **94**, 205426 (2016).
- ²⁸Q. Liu, X. Zhang, L. B. Abdalla, A. Fazzio, and A. Zunger, “Switching a normal insulator into a topological insulator via electric field with application to phosphorene,” *Nano Lett.* **15**, 1222–1228 (2015).
- ²⁹J. Kim, S. S. Baik, S. W. Jung, Y. Sohn, S. H. Ryu, H. J. Choi, B.-j. Yang, and K. S. Kim, “Two-Dimensional Dirac Fermions Protected by Space-Time Inversion Symmetry in Black Phosphorus,” *Phys. Rev. Lett.* **119**, 226801 (2017).
- ³⁰S. Adhikary, S. Mohakud, and S. Dutta, “Engineering Anisotropic Klein Tunneling in Black Phosphorene through Elemental Substitution,” *Phys. Status Solidi Basic Res.* **258**, 2100071 (2021).
- ³¹C. Wang, Q. Xia, Y. Nie, and G. Guo, “Strain-induced gap transition and anisotropic Dirac-like cones in monolayer and bilayer phosphorene,” *J. Appl. Phys.* **117**, 124302 (2015).

- ³²M. Yarmohammadi, M. Mortezaei, and K. Mirabbaszadeh, “Anisotropic basic electronic properties of strained black phosphorene,” *Phys. E Low-dimensional Syst. Nanostructures* **124**, 114323 (2020).
- ³³C. Wang, Q. Xia, Y. Nie, M. Rahman, and G. Guo, “Strain engineering band gap, effective mass and anisotropic dirac-like cone in monolayer arsenene,” *AIP Adv.* **6** (2016).
- ³⁴C. Zhong, Y. Chen, Y. Xie, Y. Y. Sun, and S. Zhang, “Semi-Dirac semimetal in silicene oxide,” *Phys. Chem. Chem. Phys.* **19**, 3820–3825 (2017).
- ³⁵B. Real, O. Jamadi, M. Milićević, N. Pernet, P. St-Jean, T. Ozawa, G. Montambaux, I. Sagnes, A. Lemaître, L. Le Gratiet, A. Harouri, S. Ravets, J. Bloch, and A. Amo, “Semi-Dirac Transport and Anisotropic Localization in Polariton Honeycomb Lattices,” *Phys. Rev. Lett.* **125**, 186601 (2020).
- ³⁶J. P. Carbotte, K. R. Bryenton, and E. J. Nicol, “Optical properties of a semi-Dirac material,” *Phys. Rev. B* **99**, 115406 (2019).
- ³⁷L. Mandhour and F. Bouhadida, “Klein tunneling in deformed $\alpha - T_3$ lattice,” (2020), [arXiv:2004.10144](https://arxiv.org/abs/2004.10144).
- ³⁸E. Illes and E. J. Nicol, “Klein tunneling in the α -T3 model,” *Phys. Rev. B* **95**, 235432 (2017).
- ³⁹K. Ghasemian, M. R. Setare, D. Jahani, and J. Najji, “Klein tunneling of semi-Dirac-like fermions in graphene,” *Europhys. Lett.* **136**, 17005 (2021).
- ⁴⁰F. Zhai and J. Wang, “Shot noise in systems with semi-Dirac points,” *J. Appl. Phys.* **116** (2014).
- ⁴¹Y. Betancur-Ocampo, F. Leyvraz, and T. Stegmann, “Electron Optics in Phosphorene pn Junctions: Negative Reflection and Anti-Super-Klein Tunneling,” *Nano Lett.* **19**, 7760–7769 (2019).
- ⁴²Y. W. Choi and H. J. Choi, “Anisotropic pseudospin tunneling in two-dimensional black phosphorus junctions,” *2D Mater.* **8**, 035024 (2021).
- ⁴³Z. Li, T. Cao, M. Wu, and S. G. Louie, “Generation of Anisotropic Massless Dirac Fermions and Asymmetric Klein Tunneling in Few-Layer Black Phosphorus Superlattices,” *Nano Lett.* **17**, 2280–2286 (2017).
- ⁴⁴S. W. Jung, S. H. Ryu, W. J. Shin, Y. Sohn, M. Huh, R. J. Koch, C. Jozwiak, E. Rotenberg, A. Bostwick, and K. S. Kim, “Black phosphorus as a bipolar pseudospin semiconductor,” *Nat. Mater.* **19**, 277–281 (2020).

- ⁴⁵Y. S. Ang, S. A. Yang, C. Zhang, Z. Ma, and L. K. Ang, “Valleytronics in merging Dirac cones: All-electric-controlled valley filter, valve, and universal reversible logic gate,” *Phys. Rev. B* **96**, 245410 (2017).
- ⁴⁶K. Saha, R. Nandkishore, and S. A. Parameswaran, “Valley-selective Landau-Zener oscillations in semi-Dirac p-n junctions,” *Phys. Rev. B* **96**, 045424 (2017).
- ⁴⁷S. Rostanzadeh and M. Sarisaman, “Charge-pseudospin coupled diffusion in semi-Dirac graphene: pseudospin assisted valley transport,” *New J. Phys.* **24**, 083026 (2022).
- ⁴⁸M. I. Katsnelson, K. S. Novoselov, and A. K. Geim, “Chiral tunnelling and the Klein paradox in graphene,” *Nat. Phys.* **2**, 620–625 (2006).
- ⁴⁹W.-Y. He, Z.-D. Chu, and L. He, “Chiral Tunneling in a Twisted Graphene Bilayer,” *Phys. Rev. Lett.* **111**, 066803 (2013).
- ⁵⁰G. Montambaux, F. Piéchon, J.-N. Fuchs, and M. O. Goerbig, “A universal Hamiltonian for motion and merging of Dirac points in a two-dimensional crystal,” *Eur. Phys. J. B* **72**, 509–520 (2009).
- ⁵¹G. Montambaux, F. Piéchon, J. N. Fuchs, and M. O. Goerbig, “Merging of Dirac points in a two-dimensional crystal,” *Phys. Rev. B* **80**, 153412 (2009).
- ⁵²A. Mawrie and B. Muralidharan, “Direction-dependent giant optical conductivity in two-dimensional semi-Dirac materials,” *Phys. Rev. B* **99**, 075415 (2019).
- ⁵³X. Zhou, W. Chen, and X. Zhu, “Anisotropic magneto-optical absorption and linear dichroism in two-dimensional semi-Dirac electron systems,” *Phys. Rev. B* **104**, 235403 (2021).
- ⁵⁴H. Y. Zhang, Y. M. Xiao, Q. N. Li, L. Ding, B. Van Duppen, W. Xu, and F. M. Peeters, “Anisotropic and tunable optical conductivity of a two-dimensional semi-Dirac system in the presence of elliptically polarized radiation,” *Phys. Rev. B* **105**, 115423 (2022).
- ⁵⁵J. Kim, S. S. Baik, S. H. Ryu, Y. Sohn, S. Park, B.-G. Park, J. Denlinger, Y. Yi, H. J. Choi, and K. S. Kim, “Observation of tunable band gap and anisotropic Dirac semimetal state in black phosphorus,” *Science*. **349**, 723–726 (2015).
- ⁵⁶S. M. Cunha, D. R. da Costa, J. M. Pereira, R. N. C. Filho, B. V. Duppen, and F. M. Peeters, “Tunneling properties in α -T3 lattices: Effects of symmetry-breaking terms,” *Phys. Rev. B* **105**, 165402 (2022).
- ⁵⁷P. V. Sriluckshmy, K. Saha, and R. Moessner, “Interplay between topology and disorder in a two-dimensional semi-Dirac material,” *Phys. Rev. B* **97**, 024204 (2018).

- ⁵⁸K. Saha, “Photoinduced Chern insulating states in semi-Dirac materials,” *Phys. Rev. B* **94**, 081103(R) (2016).
- ⁵⁹P. Zhang, “Scaling for quantum tunneling current in nano- and subnano-scale plasmonic junctions,” *Sci. Rep.* **5**, 1–11 (2015).
- ⁶⁰S. Yuan, A. N. Rudenko, and M. I. Katsnelson, “Transport and optical properties of single- and bilayer black phosphorus with defects,” *Phys. Rev. B* **91**, 115436 (2015).
- ⁶¹V. A. Khlus, “Current and voltage fluctuations in microjunctions between normal metals and superconductors,” *Sov Phys JETP* **66**, 2179–2190 (1987).
- ⁶²J. Ahn, S. Park, D. Kim, Y. Kim, and B. J. Yang, “Stiefel-Whitney classes and topological phases in band theory,” *Chinese Phys. B* **28** (2019).